Efficient Channel-Estimation-Based Multiuser Detection for Underwater CDMA Systems

Eduard Calvo, *Student Member, IEEE*, and Milica Stojanovic, *Senior Member, IEEE*

***Abstract*—Motivated by finding reduced complexity versions of the maximum-likelihood (ML) detector for highly distorted underwater channels, a multiuser detection (MUD) algorithm for joint data detection and channel estimation based on the cyclic coordinate descent method is proposed. Assuming that the data symbols are available, they are used to estimate the channel responses, which, in turn, are used to refine the symbol estimates. Adaptive estimation is performed using minimum mean square error as the overall optimization criterion. The receiver is implemented in a multichannel configuration, which provides the array processing gain necessary for many of the underwater acoustic channels. The complexity of the detection algorithm is linear in the number of receive elements and it does not depend on the modulation level of the transmitted signals. The algorithm has been tested using real data obtained over a 2-km shallow-water channel in a 20-kHz band, demonstrating good results.**

***Index Terms*—Adaptive algorithms, code-division multiple access, direct-sequence (DS) spread spectrum, multichannel combining, space-time processing, underwater acoustic communications.**

I. Introduction

EMERGING systems for ocean observation call for deployment of multiple autonomous underwater units. To enable their collaborative operation in a shared physical channel, multiple-access communications must be established. To this extent, while frequency-division multiple access (FDMA) is ruled out because of its inefficient use of the available bandwidth, the capacity of time-division multiple access (TDMA), which allows for simpler data detection mechanisms, is fundamentally limited by the underwater channel latency [1]. These facts motivate consideration of code-division multiple access (CDMA) as the multiple-access technique for use in underwater acoustic systems. A particular application of interest to this study is a network of several users operating within a footprint of a few kilometers around a base station.

In particular, we deal with the problem of multiuser data detection where the autonomous users transmit asynchronously to a common receiver equipped with a hydrophone array. Multiuser detection (MUD) techniques, instead of treating the interfering users as background noise, exploit the structure of their signals to perform joint detection of all the data streams [2]. As a result, the efficiency of the underwater channel resource utilization is increased with respect to nonautonomous network configurations (i.e., with transmissions scheduled by a centralized entity to avoid multiuser interference). Underwater acoustic channels are characterized by extended multipath propagation, fast variation of the channel impulse response, severe Doppler distortion, asynchronism, and bandwidth scarcity. To implement MUD on these channels, simplicity and performance need to be realized simultaneously.

The simplest among all MUD strategies is the matched-filter (MF) detector, which consists of a bank of filters each matched to the waveform corresponding to the spreading sequence and channel impulse response of a different user. Not exploiting any information available about the structure of the interference, the MF detector is extremely vulnerable to the near–far problem, which occurs when there is disparity in the received power of the users. On the other hand, Verdú [3] showed that optimal error probability performance (and near–far resistance) is achieved by a maximum-likelihood (ML) detector consisting of a Viterbi algorithm for maximum-likelihood sequence estimation (MLSE) operating on the outputs of the MFs, but the price to pay is a complexity scaling that is exponential in the number of users and becomes unaffordable in many practical situations.

These facts motivate the interest in finding reduced complexity detectors with good performance. For instance, in the decorrelator detector [4], the Viterbi MLSE is replaced by a linear transformation. Alternative structures that do not suffer from the near–far problem are the minimum mean square error (MMSE) linear [5], and decision feedback equalization (DFE) detectors [6]–[8], which are based on the adaptation of finite impulse response filters to track the instantaneous changes of the channel conditions. Another popular family of strategies for MUD are multistage (parallel or successive interference cancellation) techniques [2], [9]–[11], which are based on using tentative symbol decisions to remove interference from the signal of interest. They employ a bank of single-user receivers that exchange timing, power, and symbol estimates to reconstruct and subtract interference before demodulation of the desired data stream. The major disadvantage of these detectors is that they suffer from error propagation.

This paper tries to bridge the gap between affordable computational load and acceptable performance by proposing a reduced complexity multiuser detector for highly distorted underwater channels. It is based on a cyclic coordinate descent (CCD) strategy that avoids estimating the channel for each possible combination of transmitted symbols of the users, thus

Manuscript received February 02, 2006; revised August 11, 2007; accepted August 21, 2008. Current version published February 06, 2009.

Associate Editor: J. Preisig.

E. Calvo is with the Department of Signal Theory and Communications, Technical University of Catalonia (UPC), Barcelona 08034, Spain (e-mail: eduard@gps.tsc.upc.edu).

M. Stojanovic is with the Electrical and Computer Engineering Department, Northeastern University, Boston, MA 02115 USA (e-mail: millitsa@mit.edu).

Digital Object Identifier 10.1109/JOE.2008.2005355

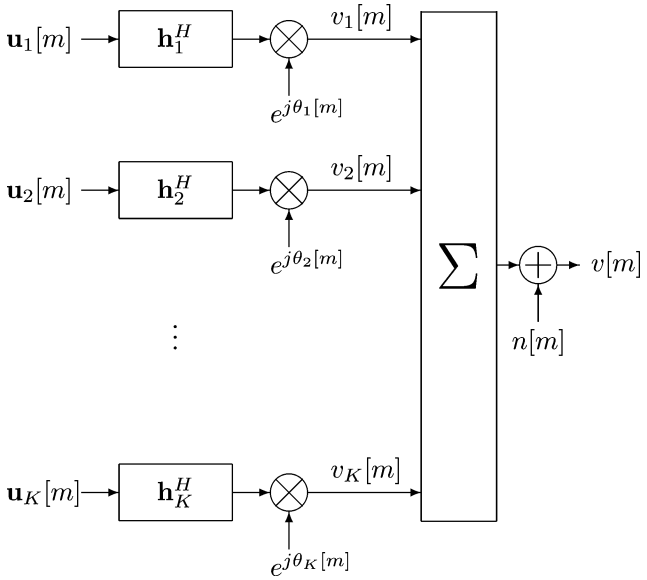

Fig. 1. Block diagram of the system.

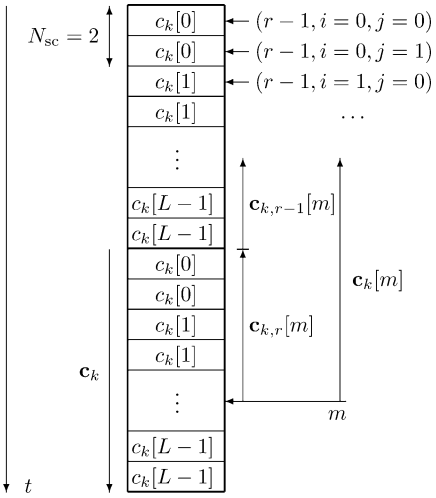

Fig. 2. Structure of the vectors $\mathbf{c}_k, \mathbf{c}_k[m]$.

reducing the computational complexity. Instead, the detector cycles through the symbol estimates, the channel estimates, and the carrier phase estimates, adjusting each one in turn while holding the other two constant. By continuously refining the three sets of parameters, channel and phase estimation only needs to be maintained for a single hypothesis on the value of the transmitted data symbols of the users, hence providing significant complexity savings.

This paper is organized as follows. Section II provides the system model. Section III describes the proposed CCD detector. Performance results of the CCD detector obtained using experimental data are given in Section IV. Finally, Section V concludes this paper.

II. System Model

We consider a direct sequence CDMA system of K users, each with the same spreading factor L (we do not consider multirate transmissions in the network). Then

$$c_k(t) = \sum_{i=0}^{L-1} c_k[i] p_c(t - iT_c) \tag{1}$$

denotes one period of the code of the kth user, where $\{c_k[i]\}_{i=0}^{L-1}$ is the spreading sequence of the kth user, T_c stands for the chip duration, and the chip shaping pulse $p_c(t)$ is taken as a squared root raised cosine pulse. In the simplest case, the overall channel as seen by the kth user is assumed to have a delay spread less than the symbol interval $T = LT_c$ (this assumption can be relaxed). Its impulse response is defined as $h_k^*(t)$, where $(\cdot)^*$ denotes a conjugate, and it is used for later convenience of notation. The sampling rate at the receiver is twice the chip rate, i.e., $N_{\rm sc} = 2$ samples per chip are used. It is useful to define the indices of symbols, chips, and samples to ease the notation for further analysis:

- current symbol index: $r \in \{0, 1, \ldots, N_d - 1\}$; N_d is the total number of transmitted data symbols per user;
- chip index within the current symbol: $i \in \{0, 1, \ldots, L-1\}$;
- sample index within the current chip of the current symbol: $j \in \{0, 1, \ldots, N_{\rm sc} - 1\}$;
- current sample index: $m \in \{0, 1, \ldots, N_d L N_{\rm sc} - 1\}$.

The relation between these indices is $m = LN_{\rm sc}r + N_{\rm sc}i + j$. To transmit the data sequence $\{d_k[r]\}_{r=0}^{N_d-1}$, the kth user forms the signal

$$u_k(t) = \sum_{r=0}^{N_d-1} d_k[r] c_k(t - rT) \tag{2}$$

which, together with the signals of the other users, is received at the base station as

$$v(t) = \sum_{k=1}^{K} v_k(t) + n(t) = \sum_{k=1}^{K} h_k^*(t) * u_k(t) e^{j\theta_k(t)} + n(t) \tag{3}$$

where $\{\theta_k(t)\}_{k=1}^K$ are the phase distortion terms and $n(t)$ is noise. An equivalent discrete-time model under a sampling rate of $N_{\rm sc}$ samples per chip is

$$\begin{aligned} v[m] &= v\left(m\frac{T_c}{N_{\rm sc}}\right) = \sum_{k=1}^{K} v_k[m] + n[m] \\ &= \sum_{k=1}^{K} \mathbf{h}_k^H[m] \mathbf{u}_k[m] e^{j\theta_k[m]} + n[m] \end{aligned} \tag{4}$$

where $(\cdot)^H$ denotes conjugate transpose. The block diagram of the system is shown in Fig. 1.

The set of channel vectors $\{\mathbf{h}_k[m]\}_{k=1}^K$ and transmitted signals $\{\mathbf{u}_k[m]\}_{k=1}^K$ have a time span of T seconds ($LN_{\rm sc}$ samples).[1] Let us define $\mathbf{c}_k$, a vector containing the $N_{\rm sc}L$ samples of one period of the code of the kth user. Then, $\mathbf{c}_k[m]$ represents a causal window of one symbol interval containing the periodic extension of the code sequence of the kth user starting at the current (mth) sample. As illustrated in Fig. 2, it is obtained by circularly shifting the vector $\mathbf{c}_k$, where the first component of

[1]In scenarios where the delay spread of the channels does not guarantee that the impulse responses are limited to one symbol interval, the definition of the vectors $\{\mathbf{u}_k[m]\}_{k=1}^K$ can be extended to include multiple symbol intervals.

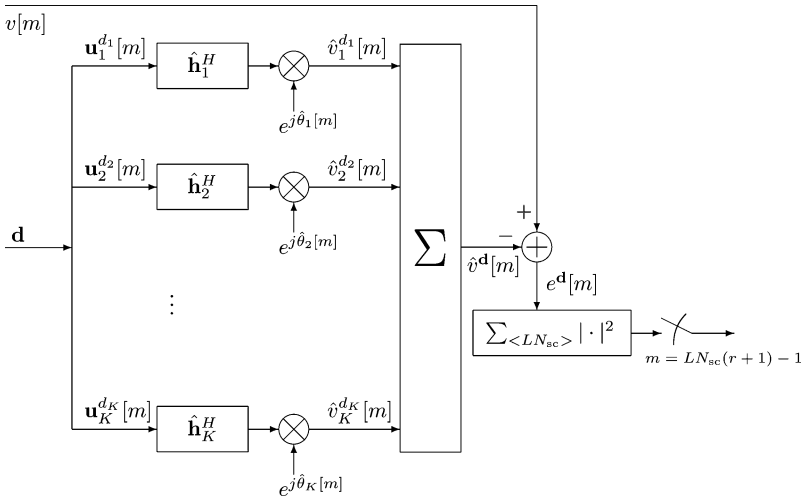

Fig. 3. Block diagram of the ML detector.

$\mathbf{c}_k[m]$ points to the $(m|_{\mathrm{mod}LN_{\mathrm{sc}}} = N_{\mathrm{sc}}i + j)$th component of $\mathbf{c}_k$

$$\mathbf{c}_k[m] = \left[\mathbf{c}_{k,r}^T[m] \quad \mathbf{c}_{k,r-1}^T[m]\right]^T. \tag{5}$$

Thus, $\mathbf{c}_k[m]$ can be split into the contribution of the current $(\mathbf{c}_{k,r}[m])$ and the past $(\mathbf{c}_{k,r-1}[m])$ code period, which allows $\mathbf{u}_k$ to be expressed as

$$\mathbf{u}_k[m] = \left[d_k[r]\mathbf{c}_{k,r}^T[m] \quad d_k[r-1]\mathbf{c}_{k,r-1}^T[m]\right]^T. \tag{6}$$

III. Data Detection

The CCD detector finds its origin in the principle of ML detection. Although it uses the same channel estimation and phase-tracking strategies as the ML detector, the way in which symbol detection is performed is very different. While the ML detector provides an upper bound on the performance of the CCD detector, it suffers from a prohibitively high computational load, which renders it infeasible for practical values of K and L. Nonetheless, we begin by describing this important algorithm as it provides the basis for the proposed CCD detector.

A. The ML Detector

Upon observing the received signal during one symbol period, the ML detector considers all the possible combinations of transmitted symbols of all the users, and decides in favor of the most likely one. That is, if $\mathcal{D}$ denotes the signal space of one user and $\mathbf{d} = [d_1 \ldots d_K]^T \in \mathcal{D}^K$ is a hypothesis made on the transmitted symbols, the decision on the rth transmitted symbol vector made by the ML detector $\widetilde{\mathbf{d}}_{\mathrm{ML}}[r]$ is

$$\widetilde{\mathbf{d}}_{\mathrm{ML}}[r] = \arg\max_{\mathbf{d}\in\mathcal{D}^K} \mathbb{P}\left(\{v[m]\}_{m=LN_{\mathrm{sc}}r}^{LN_{\mathrm{sc}}(r+1)-1} \middle| \mathbf{d}\right) \tag{7}$$

where $\mathbb{P}(\cdot)$ denoted probability. The dependence of $v[m]$ on the transmitted symbols is through the vectors $\{\mathbf{u}_k[m]\}_{k=1}^K$ given in the expression (4). Assuming that the last transmitted symbol of the kth user $d_k[r-1]$ is known,[2] $\mathbf{u}_k[m]$ (6) can be constructed up to the value of the current data symbol $d_k[r] = d$, using the knowledge of $\mathbf{c}_k[m]$ as

$$\mathbf{u}_k^d[m] \triangleq \left[d\mathbf{c}_{k,r}^T[m] \quad d_k[r-1]\mathbf{c}_{k,r-1}^T[m]\right]^T. \tag{8}$$

For each symbol $d \in \mathcal{D}$, a different vector $\mathbf{u}_k^d[m]$ can be constructed, and for each hypothesis $\mathbf{d} \in \mathcal{D}^K$, the conditional mean of the received signal is given by

$$v^{\mathbf{d}}[m] = \mathbb{E}\{v[m]|\mathbf{d}\} = \sum_{k=1}^{K} \mathbf{h}_k^H \mathbf{u}_k^{d_k}[m] e^{j\theta_k[m]} \tag{9}$$

where we have used the fact that the noise is zero mean. Because the noise is also complex Gaussian $n[m] \sim \mathcal{CN}(0, \sigma_n^2)$, this implies that $v[m]|\mathbf{d} \sim \mathcal{CN}(v^{\mathbf{d}}[m], \sigma_n^2)$, which allows us to simplify (7) as

$$\begin{aligned}
\widetilde{\mathbf{d}}_{\mathrm{ML}}[r] &= \arg\max_{\mathbf{d}\in\mathcal{D}^K} \prod_{m=LN_{\mathrm{sc}}r}^{LN_{\mathrm{sc}}(r+1)-1} \mathbb{P}(v[m]|\mathbf{d}) \\
&= \arg\max_{\mathbf{d}\in\mathcal{D}^K} \prod_{m=LN_{\mathrm{sc}}r}^{LN_{\mathrm{sc}}(r+1)-1} \frac{1}{\pi\sigma_n^2} e^{-|v[m]-v^{\mathbf{d}}[m]|^2/\sigma_n^2} \qquad (10) \\
&= \arg\min_{\mathbf{d}\in\mathcal{D}^K} \sum_{m=LN_{\mathrm{sc}}r}^{LN_{\mathrm{sc}}(r+1)-1} |v[m] - v^{\mathbf{d}}[m]|^2 \\
&\triangleq \arg\min_{\mathbf{d}\in\mathcal{D}^K} \mathsf{mse}^{\mathbf{d}}[m] \qquad (11)
\end{aligned}$$

where $\mathsf{mse}^{\mathbf{d}}[m]$ denotes the mean squared error associated with the hypothesized data sequence $\mathbf{d}$. Since $v^{\mathbf{d}}[m]$ depends on both the channel vectors and the carrier phase offsets, which are not available, an estimate $\hat{v}[m]$ will be used instead. This estimate will rely on the estimates of the channel and the carrier phases as shown in Fig. 3. Note that channel estimation and carrier phase tracking need to be carried out for each possible hypothesis, similarly as in hypothesis feedback direct sequence spread spectrum (DSSS) equalization [13], [14].

[2]More than one past symbol is required if the delay spread of the channel is longer than T.

Let $\mathbf{d}$ be the current hypothesis under test for the rth transmitted symbol vector. The estimated conditional mean is then given by

$$\hat{v}^{\mathbf{d}}[m] = \sum_{k=1}^{K} \hat{v}_k^{d_k}[m] = \left[\hat{\mathbf{h}}_1^H \ \dots \ \hat{\mathbf{h}}_K^H\right] \times \begin{bmatrix} \mathbf{u}_1^{d_1}[m]e^{j\hat{\theta}_1[m]} \\ \vdots \\ \mathbf{u}_K^{d_K}[m]e^{j\hat{\theta}_K[m]} \end{bmatrix} \triangleq \hat{\mathbf{h}}^H \mathbf{u}_\theta^{\mathbf{d}}[m]. \quad (12)$$

The composite channel estimate $\hat{\mathbf{h}}$ is updated using the normalized least mean squares (NLMS) algorithm [12], with the error signal

$$e^{\mathbf{d}}[m] = v[m] - \hat{v}^{\mathbf{d}}[m] = v[m] - \hat{\mathbf{h}}^H \mathbf{u}_\theta^{\mathbf{d}}[m]. \quad (13)$$

The phase terms $\{e^{j\hat{\theta}_k}\}_{k=1}^K$ are estimated using a multichannel digital phase-locked loop (DPLL) [8]. Due to its robustness and simplicity, a second-order DPLL is used to estimate the phase vector $\hat{\boldsymbol{\theta}}[m] = [\hat{\theta}_1[m] \ \dots \ \hat{\theta}_K[m]]^T$ using the recursive adaptation equation

$$\hat{\boldsymbol{\theta}}[m+1] = \hat{\boldsymbol{\theta}}[m] + a_1 \boldsymbol{\psi}[m] + a_2 \sum_{l \le m} \boldsymbol{\psi}[l] \quad (14)$$

where a_1, a_2 are tracking constants to be tuned (it is usual to adopt the heuristic relation $a_2 = a_1/10$) and $\boldsymbol{\psi}[m] = [\psi_1[m] \ \dots \ \psi_K[m]]^T$ is the driving signal of the DPLL, which is related to the estimation error as

$$\boldsymbol{\psi}[m] = -\frac{1}{2} \nabla_{\hat{\boldsymbol{\theta}}[m]} |e^{\mathbf{d}}[m]|^2 \quad (15)$$

or, analogously

$$\psi_k[m] = -\frac{1}{2} \frac{\partial |e^{\mathbf{d}}[m]|^2}{\partial \hat{\theta}_k[m]}, \qquad 1 \le k \le K. \quad (16)$$

By stacking the contributions of all the users to the estimated mean of the received signal $\hat{\mathbf{v}}^{\mathbf{d}}[m] = [\hat{v}_1^{d_1}[m] \ \dots \ \hat{v}_K^{d_K}[m]]^T$, a simple closed form can be obtained for $\boldsymbol{\psi}[m]$ as

$$\boldsymbol{\psi}[m] = -\mathrm{Im}\{e^{\mathbf{d}^*}[m] \hat{\mathbf{v}}^{\mathbf{d}}[m]\}. \quad (17)$$

A different filter bank and estimated phase vector is maintained for each hypothesis until the end of the current symbol period is reached, when the best hypothesis $\widetilde{\mathbf{d}}_{\mathrm{ML}}[r]$ is chosen according to (11) and the channel and phase estimates of the remaining hypotheses are then discarded. This estimator relies on the abrupt changes in the apparent channel phase that are caused by incorrect symbol assumptions. Boosting the instantaneous signal estimation error at the beginning of the symbol period, these transients result in a larger cumulated sum of errors (11) by the end of it. This trend is shown in Fig. 4. A summarized description of the overall detection process is provided in Algorithm 1,

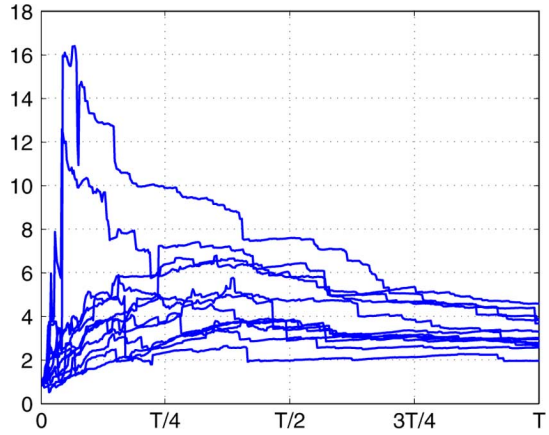

Fig. 4. Typical behavior of the transient in ML metric (sum of signal estimation errors) of an incorrect symbol assumption. The curves show the sum of errors normalized by the correct hypothesis ML metric (each curve corresponds to a different sensor).

where $\hat{\mathbf{h}}^{\mathbf{d}}$ and $\hat{\boldsymbol{\theta}}^{\mathbf{d}}$ designate the estimates associated with hypothesis $\mathbf{d}$.

Algorithm 1: ML symbol detection

1: Initialize: $\widetilde{\mathbf{d}}_{\mathrm{ML}}[-1] = \mathbf{0}_K, (\hat{\mathbf{h}}^{\mathbf{d}}, \hat{\boldsymbol{\theta}}^{\mathbf{d}}[m]) = (\mathbf{0}_{KLN_{\mathrm{sc}}}, \mathbf{0}_K) \ \forall \mathbf{d} \in \mathcal{D}^K$.
2: **for** $0 \le r \le N_d - 1$ **do**
3: **for** each $\mathbf{d} \in \mathcal{D}^K$ **do**
4: **for** $LN_{\mathrm{sc}} r \le m \le LN_{\mathrm{sc}}(r+1) - 1$ **do**
5: Get the current sample $v[m]$.
6: Update the inputs $\{\mathbf{u}_k^{d_k}[m]\}_{k=1}^K$ (8) assuming $\widetilde{\mathbf{d}}_{\mathrm{ML}}[r-1] = \mathbf{d}[r-1]$.
7: From the estimates $\{\hat{v}^{\mathbf{d}}[m], \hat{\mathbf{v}}^{\mathbf{d}}[m]\}$ (12) obtain $e^{\mathbf{d}}[m]$ (13), $\mathrm{mse}^{\mathbf{d}}[m]$, and $\boldsymbol{\psi}^{\mathbf{d}}[m]$ (17).
8: Update the channel $\hat{\mathbf{h}}^{\mathbf{d}} = \mathrm{NLMS}(e^{\mathbf{d}}[m], \mathbf{u}_\theta^{\mathbf{d}}[m])$ and phase $\hat{\boldsymbol{\theta}}^{\mathbf{d}}[m] = \mathrm{DPLL}(\boldsymbol{\psi}^{\mathbf{d}}[m])$ (14) estimates.
9: **end for**
10: **end for**
11: Decide on the symbol vector $\widetilde{\mathbf{d}}_{\mathrm{ML}}[r]$ (4).
12: Reset the filters: $(\hat{\mathbf{h}}^{\mathbf{d}}, \hat{\boldsymbol{\theta}}^{\mathbf{d}}[m]) = (\hat{\mathbf{h}}^{\widetilde{\mathbf{d}}_{\mathrm{ML}}[r]}, \hat{\boldsymbol{\theta}}^{\widetilde{\mathbf{d}}_{\mathrm{ML}}[r]}) \ \forall \mathbf{d} \ne \widetilde{\mathbf{d}}_{\mathrm{ML}}[r]$.
13: **end for**

B. The CCD Detector

As either the number of users or the size of their signal space is increased, the number of hypotheses for which the ML detector needs to maintain updated channel and phase estimates grows dramatically as $|\mathcal{D}|^K$, and it may become technically not affordable to explore all of them. The need for a simpler detector with looser complexity scalings motivates the CCD detector presented below.

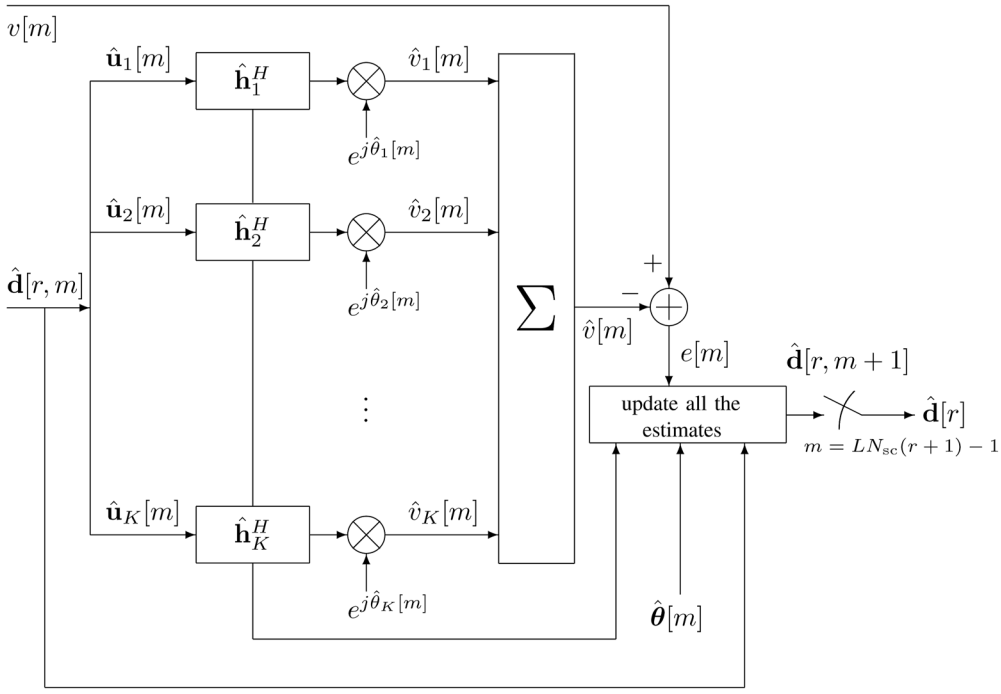

Fig. 5. Block diagram of the CCD detector.

We propose an MMSE MUD algorithm based on the CCD method [15], [16], which is an instance of Gauss–Seidel optimization. Given the problem of minimizing a multivariate cost function, the CCD method performs a descent towards a local minimum of the function by optimizing in a given (cyclic) order each of the variables (coordinates) holding the remaining ones constant. Whenever the cost function is jointly convex [17] in all the variables, this method converges to the global minimum of the function. CCD methods, however, have shown good performance in many situations that do not conform to the convexity constraint. Some applications of CCD are in tomography [18], inverse kinematics [19], bioinformatics [20], magnetic resonance imaging [21], and MUD for synchronous CDMA [22], [23].

For the problem of MMSE MUD, we identify three different variables (coordinates): the channel estimates $\hat{\mathbf{h}}$, the carrier phase offset estimates $\hat{\boldsymbol{\theta}}$, and the transmitted symbol estimates $\hat{\mathbf{d}}$. At the beginning of each symbol epoch, the CCD detector assumes an all-zeros initial value for $\hat{\mathbf{d}}$, while reliable estimates of channels and phases are assumed due to the existence of a training period at the beginning of the data packet of each user. For each sample of the received signal within the current symbol interval, the detector cycles through the following steps: the symbol estimates are refined using the recursive least squares (RLS) algorithm [12]; the channel estimates are updated using the NLMS algorithm; and the phase estimates are updated using a second-order DPLL. Whenever the last sample of a given symbol interval has been processed, symbol decision is performed by applying a regular slicer to the final symbol estimates. The structure of the CCD detector is shown in Fig. 5.

Let us denote by $\hat{\mathbf{d}}[r,m] = [\hat{d}_1[r,m] \ldots \hat{d}_K[r,m]]^T$ the estimate of the rth symbols at the mth sample. The vectors $\{\hat{\mathbf{u}}_k[m]\}_{k=1}^K$ play the same role as $\{\mathbf{u}_k^{d_k}[m]\}_{k=1}^K$ in (8), but differ in that they are built using the current symbol *estimates* and the previous *decisions* $\widetilde{\mathbf{d}}_{\mathrm{CCD}}[r-1] = [\widetilde{d}_{\mathrm{CCD},1}[r-1] \ldots \widetilde{d}_{\mathrm{CCD},K}[r-1]]^T$, i.e.,

$$\hat{\mathbf{u}}_k[m] \triangleq \left[\hat{d}_k[r,m]\mathbf{c}_{k,r}^T[m] \quad \widetilde{d}_{\mathrm{CCD},k}[r-1]\mathbf{c}_{k,r-1}^T[m]\right]^T. \tag{18}$$

Using analogous notation to denote the vertical stacking of vectors as in the previous section, the dependence of the error signal $e[m]$ on the channel and phase estimates amounts to

$$\begin{aligned} e[m] &= v[m] - \hat{v}[m] = v[m] - \sum_{k=1}^{K} \hat{\mathbf{h}}_k^H \hat{\mathbf{u}}_k[m] e^{j\hat{\theta}_k[m]} \\ &\triangleq v[m] - \hat{\mathbf{h}}^H \hat{\mathbf{u}}_\theta[m] \end{aligned} \tag{19}$$

which resembles that of the ML detector (13). Therefore, channel estimation and phase tracking can be carried out as before, using the NLMS algorithm and a second-order DPLL, respectively. A closer look at (19) shows the dependence of the error on the symbol estimates

$$\begin{aligned} e[m] &= v[m] - \sum_{k=1}^{K} \left[\hat{\mathbf{h}}_{k,r}^H \ \hat{\mathbf{h}}_{k,r-1}^H\right] \\ &\quad \times \begin{bmatrix} \hat{d}_k[r,m]\mathbf{c}_{k,r}[m] \\ \widetilde{d}_{\mathrm{CCD},k}[r-1]\mathbf{c}_{k,r-1}[m] \end{bmatrix} e^{j\hat{\theta}_k[m]} \\ &= v[m] - \underbrace{\sum_{k=1}^{K} \widetilde{d}_{\mathrm{CCD},k}[r-1]\hat{\mathbf{h}}_{k,r-1}^H \mathbf{c}_{k,r-1}[m] e^{j\hat{\theta}_k[m]}}_{\hat{v}^{r-1}[m]} \end{aligned}$$

$$
\begin{aligned}
&- \sum_{k=1}^{K} \hat{d}_k[r,m] \underbrace{\hat{\mathbf{h}}_{k,r}^H \mathbf{c}_{k,r}[m] e^{j\hat{\theta}_k[m]}}_{b_k[m]} \\
&= v[m] - \hat{v}^{r-1}[m] - [\hat{d}_1[r,m] \dots \hat{d}_K[r,m]] \begin{bmatrix} b_1[m] \\ \vdots \\ b_k[m] \end{bmatrix} \\
&\triangleq v[m] - \hat{v}^{r-1}[m] - \hat{\mathbf{d}}^T[r,m]\mathbf{b}[m]. \qquad (20)
\end{aligned}
$$

This expression gives an insight into the way in which the current and past symbol estimates affect the final estimation error: $\hat{v}^{r-1}[m]$ contains the intersymbol interference (ISI) from the previous symbols, and it is constructed relying on the correctness of $\widetilde{\mathbf{d}}_{\mathrm{CCD}}[r-1]$. After subtracting this term, the received signal $v[m]$ only contains information about the current symbol vector $\mathbf{d}[r]$. Symbol estimation can thus be performed by viewing the vector $\hat{\mathbf{d}}[r,m]$ as a filter with input $\mathbf{b}[m]$ defined in (20). This filter has to be adapted to minimize the squared error $|e[m]|^2$. Minimization of the estimation error through refinement of the symbol estimates is depicted in Fig. 6.

Since for the application at hand the number of users is not large, we use the RLS algorithm [12] to adapt the symbol estimates, because it has lower misadjustment and faster convergence than the least mean squares (LMS) algorithm. At the end of the symbol duration, the final estimate of the transmitted symbols is

$$\hat{\mathbf{d}}_{\mathrm{CCD}}[r] = \hat{\mathbf{d}}[r, LN_{\mathrm{sc}}(r+1)-1] \qquad (21)$$

over which a regular slicer can be applied to obtain the final decision, which we denote as

$$\widetilde{\mathbf{d}}_{\mathrm{CCD}}[r] = \text{decision}\,(\hat{\mathbf{d}}_{\mathrm{CCD}}[r]). \qquad (22)$$

A summary of the detection process of the CCD detector is provided in Algorithm 2, where $(\hat{\mathbf{h}}_{\mathrm{tr}}, \hat{\boldsymbol{\theta}}_{\mathrm{tr}})$ represent the channel and phase estimates obtained after the end of the training period.

Algorithm 2: CCD symbol detection

1: Initialize: $\widetilde{\mathbf{d}}_{\mathrm{CCD}}[-1] = \mathbf{0}_K, (\hat{\mathbf{h}}, \hat{\boldsymbol{\theta}}) = (\hat{\mathbf{h}}_{\mathrm{tr}}, \hat{\boldsymbol{\theta}}_{\mathrm{tr}})$.
2: **for** $0 \le r \le N_d - 1$ **do**
3: Initialization: $\hat{\mathbf{d}}[r, LN_{\mathrm{sc}}r] = \mathbf{0}_K$.
4: **for** $LN_{\mathrm{sc}}r \le m \le LN_{\mathrm{sc}}(r+1) - 1$ **do**
5: Get the current sample $v[m]$.
6: Form $\hat{\mathbf{u}}_\theta[m], e[m], v^{r-1}[m], \mathbf{b}[m]$, and $\boldsymbol{\psi}[m]$.
7: Update the symbol estimates: $\hat{\mathbf{d}}[r,m] = \mathrm{RLS}(e[m], \mathbf{b}[m])$.
8: Update the channel estimates: $\hat{\mathbf{h}} = \mathrm{NLMS}(e[m], \hat{\mathbf{u}}_\theta[m])$.
9: Update the phase estimates: $\hat{\boldsymbol{\theta}}[m] = \mathrm{DPLL}(\boldsymbol{\psi}[m])$.
10: **end for**
11: Symbol estimate: $\hat{\mathbf{d}}_{\mathrm{CCD}}[r] = \hat{\mathbf{d}}[r, m = LN_{\mathrm{sc}}(r+1) - 1]$.
12: Symbol decision: $\widetilde{\mathbf{d}}_{\mathrm{CCD}}[r] = \mathrm{slicer}(\hat{\mathbf{d}}_{\mathrm{CCD}}[r])$.
13: **end for**

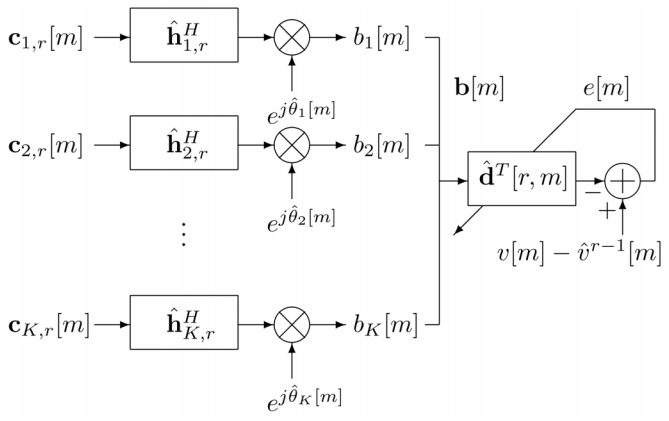

Fig. 6. Adaptive symbol estimation scheme of the CCD detector.

There are several refinements that can be added to the basic algorithm to improve its performance. These steps are listed below.

After the training period, the estimate of the received signal $\hat{v}[m]$ is computed using truncated versions of the channel estimates $\{\hat{\mathbf{h}}_k\}_{k=1}^K$ to reduce the estimation noise. All the taps of $\hat{\mathbf{h}}_k$ with an amplitude below G times the amplitude of its largest tap are set to zero. Thus, only the most significant taps (corresponding to the main arrivals of the signals) are taken into account when constructing the signal estimate. In this manner, the fact that the actual response can be sparse (which may be the case in underwater acoustic channels) is taken into account.

The forgetting factor λ of the RLS algorithm used to update the symbol estimates plays an important role in determining the final performance of the detector. While a small value of λ guarantees fast convergence, it results in large misadjustment. On the other hand, a high value of λ (a value close to 1) ensures small misadjustment at the price of slow convergence. Because the number of iterations available to the symbol estimates to converge is severely constrained (they should be accurate after adaptation during one symbol interval, which contains LN_{sc} samples), it can happen so that by the time the end of the symbol period is reached, the symbol estimates still have low amplitudes. To solve this problem, an iterative symbol estimation routine can be implemented, in which several sweeps are made over the same symbol interval. At the end of each sweep, the symbol estimates and channel parameters are saved and used to initialize the next sweep starting at the beginning of the same symbol interval. In this manner, the distance from the initial guess for the symbol estimate to its desired value is made progressively shorter, and the problem of low-amplitude symbol estimates is overcome. The price to pay is a linear increase of the computational load in the number of sweeps N_{sw}.

Last, after all the sweeps corresponding to one symbol interval have been performed and the final symbol decision has been made, an extra sweep over the same symbol interval is performed using the symbol decisions instead of the symbol estimates. Thus, channel estimation and phase tracking are performed using the discrete, admissible value $\widetilde{\mathbf{d}}_{\mathrm{CCD}}[r]$ for the symbols, resulting in improved quality of estimates, and ultimately a better performance after the training period.

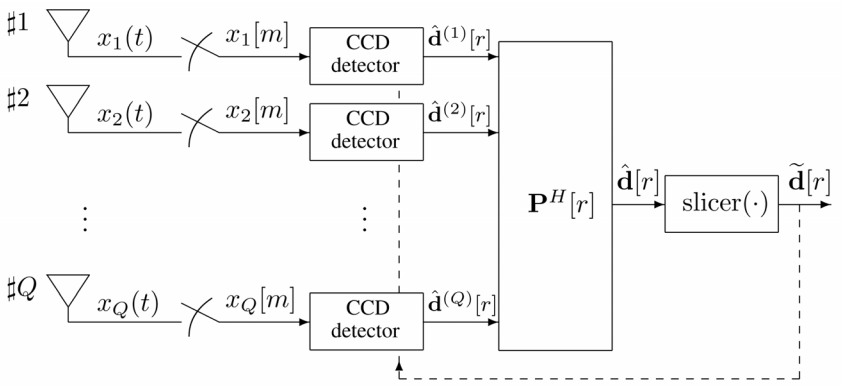

Fig. 7. Structure of the multichannel CCD detector.

C. Extension to Multichannel Receivers

If the receiver has more than one element, spatial diversity combining can offer further processing gains. In wideband underwater applications, temporal processing is needed for each of the elements, and for this reason, as many CCD detectors as there are receive array elements (Q) are used in the multichannel configuration, as shown in Fig. 7. The outputs of the detectors are MMSE combined at the end of each symbol interval. In this manner, the information from *all* the temporal processors is used to make symbol decisions that are then fed back to the detectors (dashed line of Fig. 7). Each of the CCD detectors thus uses the improved decisions made *after* spatial diversity combining to perform the last sweep over the symbol interval, and to update the vectors $\{\hat{\mathbf{u}}_k\}_{k=1}^K$.

To analyze the design of the combiner, we will drop the symbol index r for the sake of brevity. Let us denote by $\hat{\mathbf{d}}^{(q)} = [\hat{d}_1^{(q)} \dots \hat{d}_K^{(q)}]^T$ the current symbol estimates obtained by processing the signal of the qth receive element. By using the set of estimates grouped on a per-user basis $\hat{\mathbf{d}}_k \triangleq [\hat{d}_k^{(1)} \dots \hat{d}_k^{(Q)}]^T$, the final symbol estimate and the symbol decision of the kth user are, respectively

$$\hat{d}_k = \mathbf{p}_k^H \hat{\mathbf{d}}_k, \widetilde{d}_k = \text{decision}\,(\hat{d}_k) \tag{23}$$

where $\mathbf{p}_k^H$ is the kth column of the combiner $\mathbf{P} = [\mathbf{p}_1 \dots \mathbf{p}_k]$, which is designed according to the MMSE criterion as

$$\mathbf{p}_k = \arg\min_{\mathbf{p}_k} = \mathbf{E}\{|\widetilde{d}_k - \hat{d}_k|^2\}. \tag{24}$$

To obtain the optimal combining vectors $\mathbf{p}_k$, we model the symbol estimates as

$$\hat{\mathbf{d}}_k = d_k \mathbf{1}_Q + \mathbf{w}_k \tag{25}$$

where d_k is the true transmitted symbol, and $\mathbf{w}_k = [w_k^{(1)} \dots w_k^{(Q)}]^T$ is the estimation noise that is independent of d_k. Assuming that $\widetilde{d}_k = d_k$, the optimal $\mathbf{p}_k$ (24) is given by the well-known Wiener's solution

$$\mathbf{p}_k = \mathbf{R}_k^{-1} \mathbf{s}_k \tag{26}$$

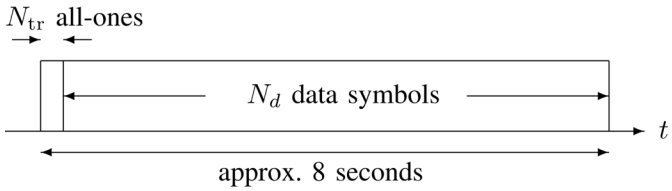

Fig. 8. Structure of a data packet.

where

$$\begin{aligned}\mathbf{R}_k &= \mathbb{E}\left\{\hat{\mathbf{d}}_k \hat{\mathbf{d}}_k^H\right\} = \underbrace{\mathbb{E}\left\{|d_k|^2\right\}}_{1} \mathbf{1}_Q \mathbf{1}_Q^H + \underbrace{\mathbb{E}\left\{\mathbf{w}_k \mathbf{w}_k^H\right\}}_{\triangleq \mathbf{R}_{\mathbf{w}_k}} \\ &= \mathbf{1}_Q \mathbf{1}_Q^H + \mathbf{R}_{\mathbf{w}_k} \qquad (27)\\ \mathbf{s}_k &= \mathbb{E}\{d_k^* \hat{\mathbf{d}}_k\} = \mathbb{E}\{d_k^*(d_k \mathbf{1}_Q + \mathbf{w}_k)\} \\ &= \mathbb{E}\left\{|d_k|^2\right\} \mathbf{1}_Q = \mathbf{1}_Q. \qquad (28)\end{aligned}$$

Note that for the assumed unit-power constant amplitude modulation, the squared modulus of a symbol does not depend on its index k. To simplify the matrix inversion in (26), Woodbury's identity[3] is used, resulting in

$$\mathbf{p}_k = \frac{\mathbf{R}_{\mathbf{w}_k}^{-1} \mathbf{1}_Q}{1 + \mathbf{1}_Q^H \mathbf{R}_{\mathbf{w}_k}^{-1} \mathbf{1}_Q}. \tag{29}$$

Further simplification is obtained from the assumption that the estimation noise from different receive elements is uncorrelated, and hence $\mathbf{R}_{\mathbf{w}_k} = \text{diag}(\{\lambda_k^{(q)}\}_{q=1}^Q)$, where $\lambda_k^{(q)} = \mathbb{E}\{|w_k^{(q)}|^2\}, 1 \le q \le Q$. Although the exact values of $\lambda_k^{(q)}$ cannot be computed due to the expectation operator, they can be estimated as

$$\hat{\lambda}_k^{(q)} = \left|\text{decision}\left(d_k^{(q)}\right) - \hat{d}_k^{(q)}\right|^2. \tag{30}$$

[3] $(\mathbf{A} + \alpha \mathbf{b}\mathbf{b}^H)^{-1} = \mathbf{A}^{-1} - (\alpha^2)/(1 + \alpha^2 \mathbf{b}^H \mathbf{A}^{-1} \mathbf{b}) \mathbf{A}^{-1} \mathbf{b}\mathbf{b}^H \mathbf{A}^{-1}$.

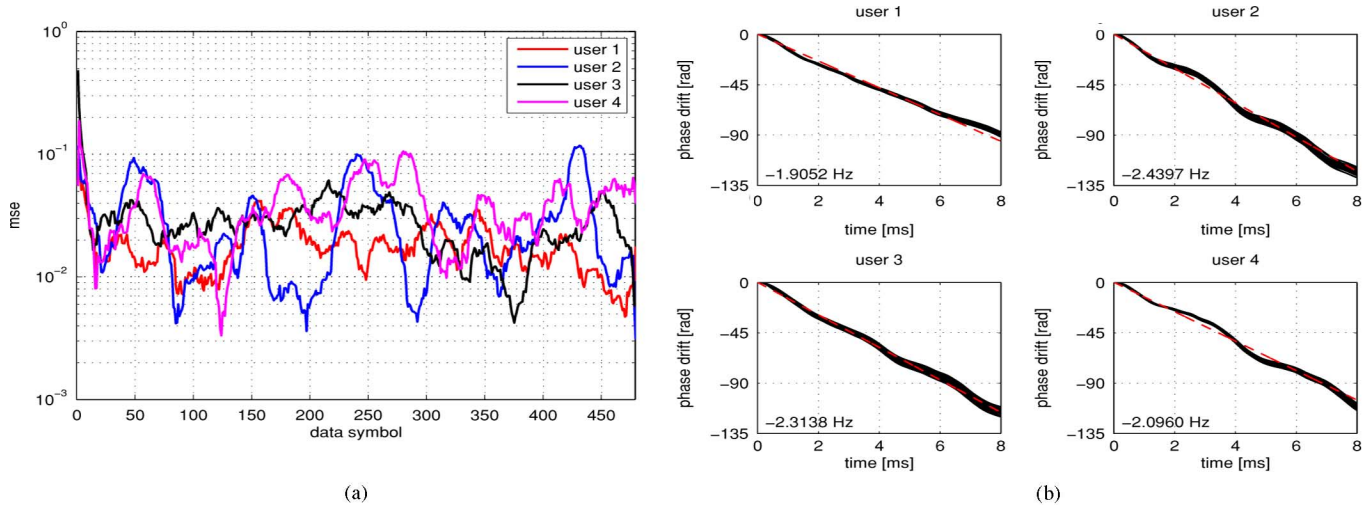

Fig. 9. (a) Normalized mse and (b) estimated carrier phase offsets for data set 1 (corresponding estimated Doppler shifts are indicated in the figure).

Thus, $\mathbf{R}_{\mathbf{w}_k}^{-1} \approx \mathrm{diag}(\{1/\hat{\lambda}_k^{(q)}\}_{q=1}^{Q})$, and the final solution exhibits dependence only on the set of error metrics $\{\hat{\lambda}_k^{(q)}\}_{q=1}^{Q}$

$$\mathbf{p}_k = \frac{1}{1+\sum_{q=1}^{Q} 1/\hat{\lambda}_k^{(q)}} \left[1/\hat{\lambda}_1^{(q)} \ldots 1/\hat{\lambda}_K^{(q)}\right]^T \tag{31}$$

$$\hat{d}_k = \frac{1}{1+\sum_{q=1}^{Q} 1/\hat{\lambda}_k^{(q)}} \sum_{q=1}^{Q} \frac{\hat{d}_k^{(q)}}{\hat{\lambda}_k^{(q)}}. \tag{32}$$

Note that the weights assigned to each component of $\hat{\mathbf{d}}_k$ depend on the quality of their associated estimates, measured in terms of $\hat{\lambda}_k^{(q)}$. The positive scaling that normalizes the right-hand side of (32) acts as an adaptive gain control that keeps the consistency of the channel estimates. The symbol decisions, made on the estimates (32), are fed back to the bank of CCD detectors and used to perform the last sweep over the symbol interval, as explained in Section III-B.

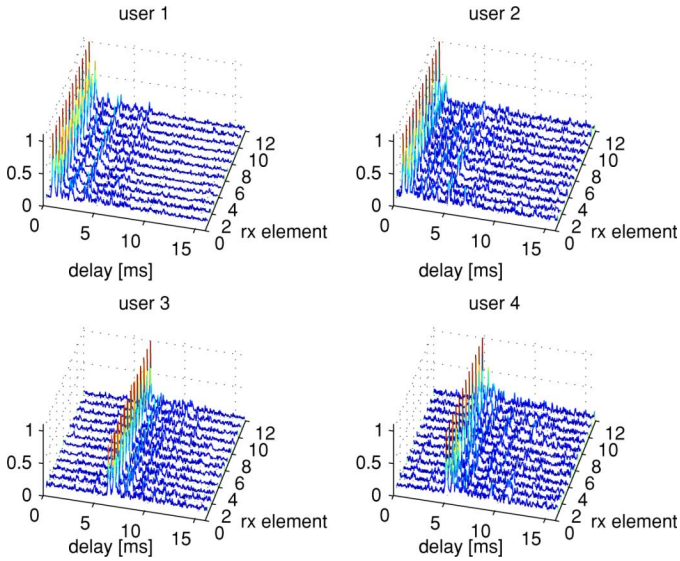

Fig. 10. Normalized channel estimates for data set 1. The delay axis spans one symbol interval.

IV. Results

The performance of the multichannel multiuser detection algorithm proposed in Sections III-B and III-C has been assessed using real data.

A. Description of the Experiment

The experimental data were recorded by the Acoustic Communications group of the Woods Hole Oceanographic Institution (Woods Hole, MA) near the island of Elba, Italy, in fall 2003. Transmission in shallow water (100-m depth) was performed over a range of 2.3 km (1.4 miles). The transmitter and the receiver were submerged at a depth of 20 and 30 m, respectively. The receiver was equipped with a vertical linear array of 12 hydrophones with a uniform spacing of 15 cm between elements. More details about the experimental deployment can be found in [14].

The signals corresponding to four users were transmitted in sequence, and the recordings were added later to simulate the multiuser effect. Due to the constraints of the deployment, the signals were transmitted from approximately the same location. Consequently, there is less channel diversity between the users than there would be in an actual system. This makes the multiuser detection more difficult, as the natural channel diversity can greatly help the receiver in distinguishing between the users [24]. Also, by adding the signals after-the-fact, more noise is introduced into the detection process. Nonetheless, recording the signals individually allows one to experiment with a varying number of users, i.e., varying levels of multiple-access interference.

The transmission of each user consisted of a single data packet up to 8 s long. Each data packet (Fig. 8) contained a training sequence followed by an information block. The training sequence was a burst of N_{tr} all-one symbols producing an overhead of roughly 4%. These symbols are intended for the acquisition of initial channel and phase estimates before data detection begins.

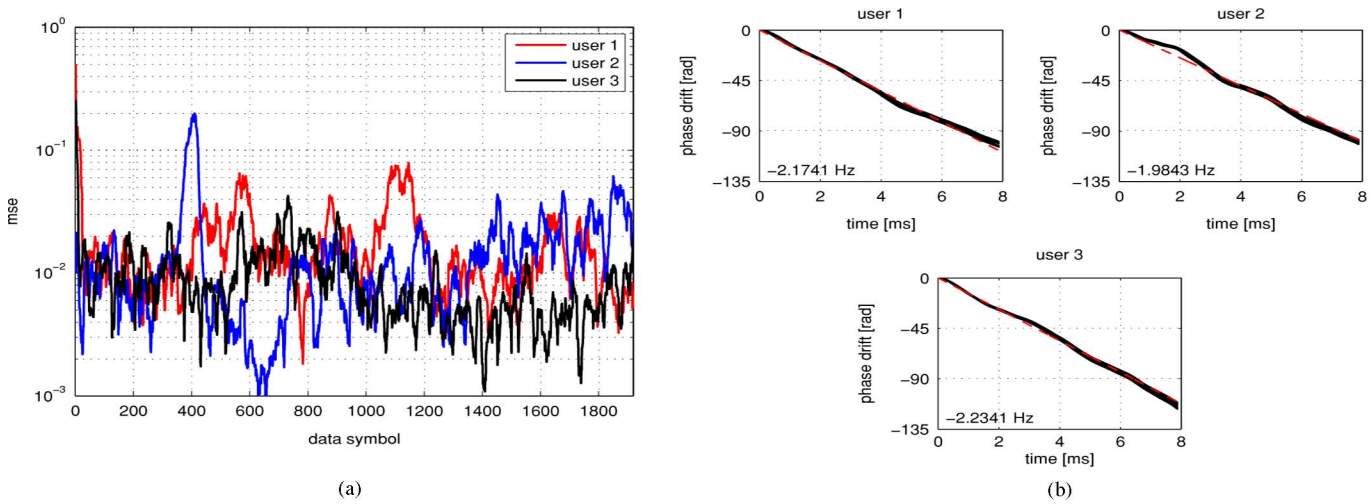

(a) (b)

Fig. 11. (a) Normalized mse and (b) estimated carrier phase offsets for data set 1 (corresponding estimated Doppler shifts are indicated in the figure).

TABLE I
PACKET STRUCTURE AND ACHIEVABLE DATA RATES FOR THE REPORTED CONFIGURATIONS

data set	L	T	packet duration	N_{tr}	N_d	net data rate
1	255	15.9375 ms	7.97 s	20	480	120 b/s/user
2	63	3.9375 ms	7.88 s	80	1920	487 b/s/user
3	15	0.9375 ms	7.50 s	320	7680	2048 b/s/user

TABLE II
PARAMETERS OF THE CCD DETECTOR

data set	L	N_{sc}	μ	λ	a_1	a_2	N_{sw}	G
1	255	2	0.2	0.999	0.1	0.01	1	0.25
2	63	2	0.05	0.999	0.1	0.01	3	0.25
3	15	2	0.1	0.999	0.1	0.01	10	0.25

The received signals were added in an asynchronous manner, i.e., each signal was delayed randomly within an interval $[0, T]$ before addition. The modulation used by all the users was quaternary phase-shift keying (QPSK) and the chip rate was 16 000 chips/s. DSSS modulation was implemented using the Kasami sequences [25] of length 255, 63, and 15, resulting in three different data sets (labeled 1, 2, and 3, respectively). The received signals were digitally down-converted to baseband and sampled at twice the chip rate ($N_{\mathrm{sc}} = 2$). The carrier frequency was 35 kHz, and raised cosine pulses with roll-off factor 0.25 were used for chip shaping within the transmission bandwidth 25 and 45 kHz. The achieved data rates and other relevant system parameters are listed in Table I. The parameters of the multichannel CCD detector used to process the different data sets are summarized in Table II, where μ denotes the step size of the NLMS algorithm employed to adapt the channel estimates and λ denotes the forgetting factor of the RLS algorithm used to adapt the symbol estimates.

B. Performance Evaluation

Results of data processing using all the receive elements ($Q = 12$) of the array are shown in Figs. 9–13. Shown are the following performance measures: the mean square error

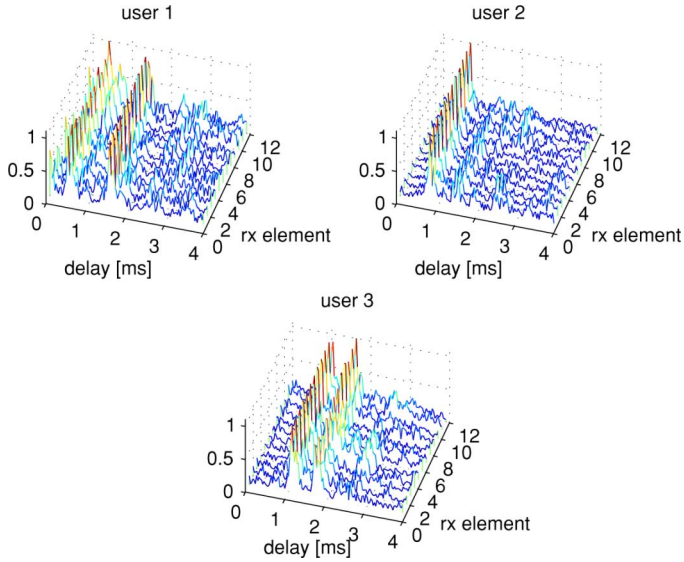

Fig. 12. Normalized channel estimates for data set 2. The delay axis spans one symbol interval.

$\mathsf{mse}_k[r]$ between the true and estimated (32) data symbols of each user, i.e.,

$$\mathsf{mse}_k[r] = |\hat{d}_k[r] - d_k[r]|^2, \tag{33}$$

the estimated carrier phase offsets, and the estimated channel impulse responses at each receive element at the end of the training period. The normalized mse values were lowpass filtered with a moving average of length ten symbols. The tracked phase offsets are shown together with a linear fit whose slope is indicated in the plots as the estimated Doppler shift.

Four users are combined in the data set 1, where the spreading factor was $L = 255$, and the aggregate throughput was 480 b/s. This is the configuration with maximal interference rejection capabilities due to the long period of the spreading codes. The mse stayed below -10 dB throughout detection [Fig. 9(a)] and the data packets of all four users were detected without errors. Doppler shifts of a few hertz were measured from the estimated

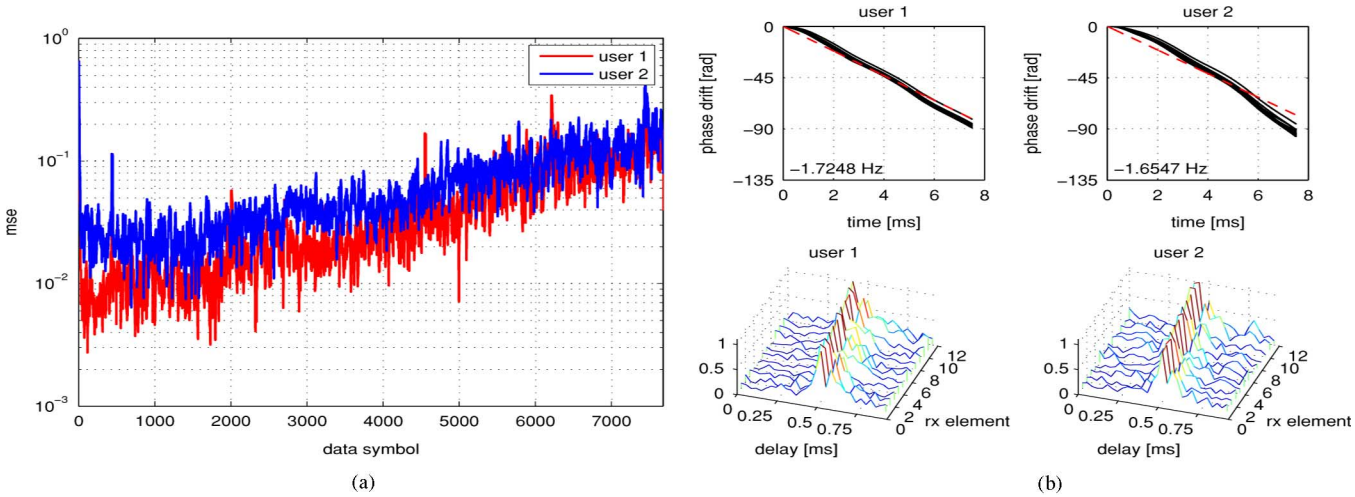

Fig. 13. (a) Normalized mse and (b, top row) estimated carrier phase offsets for data set 3 (corresponding estimated Doppler shifts are indicated in the figure). The delay axis of the (b, bottom row) normalized channel estimate plots spans one symbol interval.

carrier phase offsets as shown in the Fig. 9(b). The estimated channel responses, shown in Fig. 10, concentrate most of their energy in a time span of about 7 ms, which fits well within one symbol interval (≈16 ms for this data set). Although we only report on the results obtained when all the receive elements were processed, we have observed that as few as four array elements (when chosen maximally spaced) suffice to provide error-free performance for this packet transmission.

The scenario under study in data set 2, where the spreading factor was $L = 63$, is that of three simultaneous users resulting in an aggregate throughput of 1.46 kb/s. The data packets of the three users were decoded with no errors, which required $N_{\text{sw}} = 3$ sweeps to compensate for the reduction in the length of the period of the spreading codes as compared to the data set 1. Fig. 11(a) shows the mse's, and, although no detection errors were produced, performance degradation with respect to the case $L = 255$ can be appreciated. The computed Doppler shifts and tracked carrier phase offsets are shown in Fig. 11(b). The estimated channel responses, shown in Fig. 12, fit tightly within one symbol period. This may explain the fact that error-free detection of four users could not be supported in this setup. Error-free performance with three simultaneous users is achieved with four receive elements (chosen maximally spaced).

The processing of the signals of data set 3, where the spreading factor was $L = 15$, was the most difficult because there is the least interference rejection capability in this case. The reduction of the spreading factor has a direct impact on the symbol estimates, which need to become reliable with a few updates. The necessary number of sweeps in this case was $N_{\text{sw}} = 10$. Using all 12 receive elements, an acceptable probability of error was achieved for two users transmitting at an aggregate rate of 4 kb/s (3.8×10^{-3} and 0.13, respectively). Fig. 13(a) shows the mse, which suffers from increasing degradation. This figure suggests that performance could be boosted by refreshing the training period after the first half of the packet. While the tracked carrier phase offset shows good performance, the channel estimates of Fig. 13(b) (bottom row) show that we are only able to capture the main arrival within one symbol period. This is an additional factor that limits the performance at $L = 15$.

MF at symbol rate was also explored as a benchmark. In particular, we considered matching the filter of each user to its overall signature (after convolution with the channel impulse response) and phase tracking in the form of a second-order DPLL. In any of the data sets, the performance of symbol-rate adaptive detection was not acceptable, yielding for instance a 10-dB loss in output signal-to-noise ratio (SNR) as compared to the CCD detector when processing one user of data set 1. While with small values of the spreading factor performance is hampered by large ISI, with large values of the spreading factor, the main impairment is fast channel variation over a symbol period. In essence, the CCD detector deals with these issues by going down to chip-rate adaptation and considering the interference created by the previous symbol.

V. Conclusion

Simultaneous transmission by multiple users is of interest for underwater sensor networks, where slowly time-varying parameters are monitored, and also for event detection in fixed networks with loose rate requirements. Multiple access based on code division is considered as a candidate technique for such a system, and an adaptive MUD for DS-CDMA has been proposed. The detector is based on the computationally affordable CCD method to optimize the detection performance under the MMSE criterion.

The proposed multichannel CCD detector has been successfully tested using real data from the recordings of underwater DS-CDMA signals. Three different data sets have been processed, each corresponding to a different value of the period of the spreading codes. Not surprisingly, the best results are achieved with the longest codes. This is because the longer codes provide greater interference cancellation capability but they also imply a longer symbol period (assuming that the chip duration is kept constant so as to utilize all of the available bandwidth), which loosens the constraints on the time given to the symbol estimates to be reliable. Finally, because we have

chosen to estimate the channel out to one symbol duration, the underlying assumption that the delay spread is limited to one symbol interval becomes violated as the symbol duration decreases at low spreading factor, eventually causing a degradation in performance. However, this degradation is not inherent to the CCD detector, and it can be overcome simply by designing the channel estimator to include as many symbol intervals as necessary.

REFERENCES

[1] F. Salvà-Garau and M. Stojanovic, "Multi-cluster protocol for ad-hoc mobile underwater acoustic networks," in *Proc. IEEE OCEANS Conf.*, Sep. 2003, vol. 1, pp. 91–98.

[2] S. Verdú, *Multiuser Detection*. Cambridge, U.K.: Cambridge Univ. Press, 1998.

[3] S. Verdú, "Minimum probability of error for asynchronous Gaussian multiple-access channels," *IEEE Trans. Inf. Theory*, vol. IT-32, no. 1, pp. 85–96, Jan. 1986.

[4] R. Lupas and S. Verdú, "Linear multiuser detectors for synchronous code-division multiple-access channels," *IEEE Trans. Inf. Theory*, vol. 35, no. 1, pp. 123–136, Jan. 1989.

[5] U. Madhow, "MMSE interference suppression for timing acquisition and demodulation in direct-sequence CDMA systems," *IEEE Trans. Commun.*, vol. 46, no. 8, pp. 1065–1075, Aug. 1998.

[6] L. M. Chen and B. S. Chen, "A robust adaptive DFE receiver for DS-CDMA systems under multipath fading channels," *IEEE Trans. Signal Process.*, vol. 49, no. 7, pp. 1523–1532, Jul. 2001.

[7] M. Majmundar, N. Sandhu, and J. H. Reed, "Adaptive single-user receivers for direct-sequence spread spectrum CDMA systems," *IEEE Trans. Veh. Technol.*, vol. 49, no. 2, pp. 379–389, Mar. 2000.

[8] M. Stojanovic and Z. Zvonar, "Multichannel processing of broad-band multiuser communication signals in shallow water acoustic channels," *IEEE J. Ocean. Eng.*, vol. 21, no. 2, pp. 156–166, Apr. 1996.

[9] Y. F. Huang, J. H. Wen, and H. T. Wu, "An adaptive decision-feedback multiuser detector using parallel interference cancellation for CDMA systems," in *Proc. IEEE Veh. Technol. Conf. Spring*, May 2001, vol. 3, pp. 1770–1774.

[10] H. K. Yeo, B. S. Sharif, A. E. Adams, and O. R. Hinton, "Performances of multi-element multi-user detection strategies in a shallow-water acoustic network (SWAN)," *IEEE J. Ocean. Eng.*, vol. 26, no. 4, pp. 604–611, Oct. 2001.

[11] H. K. Yeo, B. S. Sharif, A. E. Adams, and O. R. Hinton, "Implementation of multiuser detection strategies for coherent underwater acoustic communication," *IEEE J. Ocean. Eng.*, vol. 27, no. 1, pp. 17–27, Jan. 2002.

[12] S. S. Haykin, *Adaptive Filter Theory*. Englewood Cliffs, NJ: Prentice-Hall, 2001.

[13] F. Blackmon, E. Sozer, M. Stojanovic, and J. Proakis, "Performance comparison of RAKE and hypothesis feedback direct sequence spread spectrum techniques for underwater communication applications," in *Proc. MTS/IEEE OCEANS Conf.*, Oct. 2002, vol. 1, pp. 594–603.

[14] M. Stojanovic and L. Freitag, "Multichannel detection for wideband underwater acoustic CDMA communications," *IEEE J. Ocean. Eng.*, vol. 31, no. 3, pp. 685–695, Jul. 2006.

[15] D. G. Luenberger, *Linear and Nonlinear Programming*, 2nd ed. Reading, MA: Addison-Wesley, 1989, pp. 227–232.

[16] W. L. Briggs, V. E. Henson, and S. F. McCormick, *A Multigrid Tutorial*. Philadelphia, PA: SIAM, 2000.

[17] S. Boyd and L. Vandenberghe, *Convex Optimization*. Cambridge, U.K.: Cambridge Univ. Press, 2004.

[18] C. A. Bouman and K. Sauer, "A unified approach to statistical tomography using coordinate descent optimization," *IEEE Trans. Image Process.*, vol. 5, no. 3, pp. 480–492, Mar. 1996.

[19] C. Welman, "Inverse kinematics and geometric constraints for articulated figure manipulation," M.S. thesis, Schl. Comput. Sci., Simon Fraser Univ., Burnaby, BC, Canada, Sep. 1993.

[20] A. A. Canutescu and R. L. Dunbrack Jr., "Cyclic coordinate descent: A robotics algorithm for protein loop closure," *Protein Sci.*, vol. 12, pp. 963–972, May 2003.

[21] W. S. Hoge, E. L. Miller, H. Lev-Ari, D. H. Brooks, W. C. Karl, and L. P. Panych, "An efficient region of interest acquisition method for dynamic magnetic resonance imaging," *IEEE Trans. Image Process.*, vol. 10, no. 7, pp. 1118–1128, Jul. 2001.

[22] J. Luo, G. Levchuk, K. Pattipati, and P. Willett, "A class of coordinate descent methods for multiuser detection," in *Proc. IEEE Int. Conf. Acoust. Speech Signal Process.*, Jun. 2000, vol. 5, pp. 2853–2856.

[23] F. Hasegawa, J. Luo, K. Pattipati, P. Willett, and D. Pham, "Speed and accuracy comparison of techniques for multiuser detection in synchronous CDMA," *IEEE Trans. Commun.*, vol. 52, no. 4, pp. 540–545, Apr. 2004.

[24] M. Stojanovic and L. Freitag, "Multiuser undersea acoustic communications in the presence of multipath propagation," in *Proc. IEEE OCEANS Conf.*, Honolulu, HI, Nov. 2001, vol. 4, pp. 2165–2169.

[25] D. V. Sarwate and M. B. Pursley, "Cross correlation properties of pseudorandom and related sequences," *Proc. IEEE*, vol. 68, no. 5, pp. 593–620, May 1980.

Eduard Calvo (S'02) received the electrical engineering degree (with highest honors) from the Telecom Barcelona School, Technical University of Catalonia (UPC), Catalonia, Spain, in 2004, where he is currently working towards the Ph.D. degree at the Department of Signal Theory and Communications.

Since 2005 he has been the recipient of a Spanish Ministry of Education and Science Research Grant at the Department of Signal Theory and Communications, UPC, where he has participated in several European projects such as IST-ROMANTIK (2003–2004), IST-SURFACE (2006–2008), and IST-FIREWORKS (2006–2008). During 2004 and 2008, he held research appointments at the Massachusetts Institute of Technology, Cambridge. His research interests lie in the intersection of information theory, optimization theory, statistical signal processing, and their applications to mobile radio and underwater acoustic communication networks.

Mr. Calvo received the Salvà i Campillo award for the Best Young Engineer by the College of Electrical Engineers of Catalonia in 2005.

Milica Stojanovic (S'90–M'93–SM'08) graduated from the University of Belgrade, Belgrade, Serbia, in 1988, and received the M.S. and Ph.D. degrees in electrical engineering from Northeastern University, Boston, MA, in 1991 and 1993, respectively.

After a number of years with the Massachusetts Institute of Technology (MIT), where she was a Principal Scientist, in 2008, she joined the faculty of Electrical and Computer Engineering Department at Northeastern University. She is also a Guest Investigator at the Woods Hole Oceanographic Institution, Woods Hole, MA, and a Visiting Scientist at MIT. Her research interests include digital communications theory, statistical signal processing and wireless networks, and their applications to mobile radio and underwater acoustic communication systems.

Dr. Stojanovic is an Associate Editor of the IEEE JOURNAL OF OCEANIC ENGINEERING.